Magnetic Resonance in Medicine 62:717–730 (2009)

Free Water Elimination and Mapping from Diffusion MRI

Ofer Pasternak,[1*] Nir Sochen,[2] Yaniv Gur,[2] Nathan Intrator,[1] and Yaniv Assaf[3,4]

Relating brain tissue properties to diffusion tensor imaging (DTI) is limited when an image voxel contains partial volume of brain tissue with free water, such as cerebrospinal fluid or edema, rendering the DTI indices no longer useful for describing the underlying tissue properties. We propose here a method for separating diffusion properties of brain tissue from surrounding free water while mapping the free water volume. This is achieved by fitting a bi-tensor model for which a mathematical framework is introduced to stabilize the fitting. Applying the method on datasets from a healthy subject and a patient with edema yielded corrected DTI indices and a more complete tract reconstruction that passed next to the ventricles and through the edema. We were able to segment the edema into areas according to the condition of the underlying tissue. In addition, the volume of free water is suggested as a new quantitative contrast of diffusion MRI. The findings suggest that free water is not limited to the borders of the brain parenchyma; it therefore contributes to the architecture surrounding neuronal bundles and may indicate specific anatomical processes. The analysis requires a conventional DTI acquisition and can be easily merged with existing DTI pipelines. Magn Reson Med 62: 717–730, 2009. © 2009 Wiley-Liss, Inc.

Key words: diffusion; brain; edema; partial volume; DTI; MRI

Diffusion imaging is an MRI technique sensitive to the mean displacement of water molecules along a specified direction (1). Within typical experimental diffusion times (a few tens of milliseconds) water molecules in brain tissue are expected to have a mean displacement on the order of 5–10 μm, reflecting the degree of hindrance by surrounding cellular structures. The most common method for inferring tissue macroscopic geometry from water displacement is diffusion tensor imaging (DTI) (2), which models displacements in multiple directions using a diffusion tensor. The geometry is inferred from DTI indices (3) such as: fractional anisotropy (FA), which provides good segmentation of white matter and an indication of white matter coherence; the principal eigenvector of the tensor, which provides the orientation of white matter bundles; and the mean diffusivity (MD) or apparent diffusion coefficient (ADC), which provides a contrast mechanism for identifying areas with increased bulk diffusivity that may represent an increase in tissue water content. DTI indices have proven to have significant value both in clinical evaluation and brain research (4), including the unique ability to delineate neuronal fibers via tractography (5).

Free water is defined as water molecules that do not experience flow and are not restricted by their surroundings. In the human brain, free water is found as cerebrospinal fluid (CSF) confined to the ventricles and around the brain parenchyma. Free water may also accumulate in the form of vasogenic edema within the brain parenchyma in the extracellular space due to processes such as tumors, brain trauma, or hemorrhage that cause ruptures in the blood–brain barrier (6–8). Free water can be identified by DTI since it shows isotropic diffusion with ADC of about $3 \cdot 10^{-3}$ mm^2/s for 37°C, almost 4 times larger than the typical ADC values of the brain parenchyma (9).

The DTI indices may be regarded as tissue-specific as long as image voxels contain a single type of tissue. But when partial volume of different diffusion compartments occurs, the DTI indices reflect the weighted average of all compartments and can no longer be regarded as markers for a specific tissue (10). CSF contamination is a particular type of partial volume effect that occurs along the contour lines of the ventricles and around the perimeters of the brain parenchyma in voxels shared by CSF and brain tissue (11,12). As a result, CSF-contaminated voxels have elevated ADC and decreased FA values. A white matter voxel contaminated by free water will most probably be fitted with a relatively isotropic diffusion tensor, precluding it from being assigned as white matter. CSF contamination has been shown to affect the delineation of fibers that pass near the ventricles, such as the fornix, the cingulum, and parts of the corpus callosum (12–14), and to be a limitation in voxel-based and histogram analysis comparisons of DTI-related quantities (15). Edema has a similar effect as CSF contamination, although its location and spread depend on the localization of the pathology that caused it. In addition, edema usually infiltrates brain tissue, contaminating large areas with partial volume effects that render it impossible to identify the infiltrated tissue condition and to perform an analysis such as tractography (4,16).

Proposed methods for eliminating CSF contamination usually use the fluid-attenuated inversion recovery diffusion-weighted imaging (FLAIR-DWI) sequence that suppresses the CSF signal (12–14). However, FLAIR-DWI has several drawbacks: it usually does not correct edema contamination (due to different relaxation times), it suffers from low signal-to-noise ratio (SNR), increases scan time, increases specific absorption rate (SAR), and does not allow gating according to the cardiac cycle necessary to

[1]Blavatnik School of Computer Science, Raymond and Beverly Sackler Faculty of Exact Sciences, Tel Aviv University, Tel Aviv, Israel.

[2]Department of Applied Mathematics, Raymond and Beverly Sackler Faculty of Exact Sciences, Tel Aviv University, Tel Aviv, Israel.

[3]Department of Neurobiology, George S. Wise Faculty of Life Sciences, Tel-Aviv University, Tel Aviv, Israel.

[4]Wohl Institute for Advanced Imaging, Tel Aviv Sourasky Medical Center, Tel Aviv, Israel.

Grant sponsor: Edersheim-Levi-Gitter Institute Functional Human Brain Mapping Unit of Tel Aviv University (to O.P.); Grant sponsor: Adams Super Center for Brain Studies of Tel Aviv University (to N.S.); Grant sponsor: Israel Science Foundation; Grant number: 1280/04 (to Y.A.).

*Correspondence to: Ofer Pasternak, School of Computer Science, The Raymond and Beverly Sackler Faculty of Exact Sciences, Tel Aviv University, Tel Aviv 69978, Israel. E-mail: oferpas@post.tau.ac.il

Received 4 December 2008; revised 18 March 2009; accepted 26 March 2009.

DOI 10.1002/mrm.22055

Published online 21 July 2009 in Wiley InterScience (www.interscience.wiley.com).

prevent pulsation artifacts and misalignment (14,17). Pierpaoli and Jones (18) introduced a model-based approach for eliminating CSF contamination from conventional diffusion images. They suggested that vasogenic edema has diffusion properties similar to free water and causes similar partial volume effects as CSF contamination; in both cases free water dominates the signal attenuation, canceling out the specificity of the derived DTI indices for the underling tissue (white or gray matter). It was thus proposed that minimizing CSF contamination might also reduce the effect of edema on the signal attenuation. Pierpaoli and Jones used a bi-tensor model (11,19) that has two compartments: a free water compartment characterized by isotropic tensor with diffusivity of free water, and a tissue compartment modeled by a diffusion tensor. However, as will be shown here, the fitting problem of the bi-tensor model is ill-posed. Pierpaoli and Jones (18) suggested increasing the number of measurements and diffusion weightings (b-values) at the cost of increased scan time in order to improve the bi-tensor estimation.

In this article we describe a method that results in tissue-specific indices for free water-contaminated voxels by incorporating free water elimination in the conventional diffusion modeling pipeline. The bi-tensor model is used with tensor elements restricted to show piece-wise smoothness with diffusivities in the range expected for water molecules hindered by brain tissue. This is accomplished by adding constraints to the bi-tensor model using a variational framework and a tensor regularization scheme. Other constraints restrict the volume of the water compartment. In addition to corrected diffusion indices, we obtain a voxel-wise map of the amount of free water, which is suggested as a new contrast mechanism that may have clinical significance. The main advantages of the proposed method are that it maps and corrects free water contamination for the standard, widely used DTI acquisition schemes; the corrected tissue-specific tensor elements supply additional information on the properties of the underlying tissue and can be used for any DTI postprocessing. We demonstrate free water elimination and mapping on diffusion data of a healthy volunteer and of a patient suffering from a brain tumor surrounded by edema, and compare the results with those obtained by conventional DTI.

THEORY

Bi-tensor Model

Definition

The bi-tensor model predicts the signal attenuation factor (hereafter referred as attenuation) for free water contamination. It is the sum of attenuations contributed by two compartments: one that models free water, $\mathbf{C}_{\text{water}}$, and a tissue compartment, $\mathbf{C}_{\text{tissue}}$, that models either gray matter or a single bundle of white matter (11,19):

$$\mathbf{A}_{\text{bi-tensor}}(\mathbf{D},f) = \mathbf{C}_{\text{tissue}} + \mathbf{C}_{\text{water}} = f\mathbf{A}_{\text{tissue}}(\mathbf{D}) + (1-f)\mathbf{A}_{\text{water}}. \quad [1]$$

In Eq. [1] the voxel-wise modeled attenuation vector, $\mathbf{A}_{\text{bi-tensor}}$, has an entry for each diffusion orientation (or applied gradient direction). The compartments are represented by the modeled attenuation vectors $\mathbf{A}_{\text{tissue}}$ and $\mathbf{A}_{\text{water}}$. The scalar f is the fractional volume of the tissue compartment ($0 < f \leq 1$). The tissue compartment follows DTI's formalism (3), where the attenuation is parameterized by a diffusion tensor, $\mathbf{D}$ as:

$$[\mathbf{A}_{\text{tissue}}(\mathbf{D})]_k = \exp(-b\mathbf{q}_k^{\mathrm{T}}\mathbf{D}\mathbf{q}_k) \quad [2]$$

with b as the diffusion weightings, and $\mathbf{q}_k$ as the k'th applied gradient orientation. The k'th entry in a vector is denoted as $[\cdot]_k$. The free water compartment is modeled by a degenerate case of the DTI model, where an isotropic diffusion tensor, i.e., a scalar, d, represents the bulk diffusivity. As such, all entries of the vector $\mathbf{A}_{\text{water}}$ are equal:

$$[\mathbf{A}_{\text{water}}]_k = \exp(-bd). \quad [3]$$

The value d is fixed to the ADC of free water (in our case $d = 3 \cdot 10^{-3}$ mm^2/s for water at 37°C) (18).

The bi-tensor model is the simplest model accounting for both diffusion anisotropy and partial volume, and is a special case of the multiple tensors model (Appendix A1). Thus, it is assumed that there is no exchange of water molecules between the two compartments. Finding the parameters f and $\mathbf{D}$ that best fit Eq. [1] gives us the relative volume of each compartment and with a tensor describing geometric features of the tissue compartment. This tensor can then be used to provide tissue-specific quantities with any measure or analysis that is applicable for DTI (such as FA, ADC, and tractography). However, finding the parameters f and $\mathbf{D}$ is not trivial, as explained next.

Finding the Bi-tensor Parameters

The inverse problem of fitting the bi-tensor model is defined as finding the parameters f and $\mathbf{D}$ that minimize the distance between the modeled attenuation $\mathbf{A}_{\text{bi-tensor}}$ to the measured attenuation, $\widehat{\mathbf{A}}$ (for a chosen differences metric such as the root mean square difference). The measured attenuation, $[\widehat{\mathbf{A}}]_k = \mathbf{S}_k/\mathbf{S_0}$, is a vector containing the diffusion weighted images (DWIs), $\mathbf{S}_k$ ($k > 0$), normalized by the signal acquired for zero diffusion weightings, $\mathbf{S}_0$. This inverse problem is very similar to the inverse problem of fitting the DTI model, where the goal is to find the tensor $\mathbf{D}$ that minimizes the distance between $\mathbf{A}_{\text{tissue}}$ and $\widehat{\mathbf{A}}$. However, there is a crucial difference between the two problems: While the DTI inverse problem has a single solution (20), the bi-tensor inverse problem usually does not. This can be shown by observing Eq. [1] and noting that given f, the following quantity can be calculated:

$$\widehat{\mathbf{A}}_t = \frac{\widehat{\mathbf{A}} - \mathbf{C}_{\text{water}}}{f}. \quad [4]$$

The quantity above can be regarded as the corrected signal attenuation, or the attenuation that would have been measured for the tissue compartment had it been the only compartment. In the simplest case of six sensitizing diffusion gradients, there are infinite solutions for the bi-tensor inverse problem: There is a linear set of equations that

Table 1
A Six Gradient-Direction Synthetic Signal Attenuation Free of Noise for a Tensor with Eigenvalues 1.5 0.4 and 0.4 Is Fitted with a Range of Volume Fraction Parameters, *f*

	D			
f	λ_1	$\lambda_{2,3}$,s	ADC	FA
1	1.5	0.4	0.766667	0.686161
0.9	1.4129	0.302	0.6723	0.752622
0.8	1.3138	0.1917	0.565733	0.836464
0.7	1.1993	0.0657	0.443567	0.942394
0.6	1.0664	-0.0808	–	–
0.5	0.9017	-0.2555	–	–
0.4	0.6985	-0.4709	–	–

The columns are the obtained principal eigenvalue (λ_1), the minor eigenvalue ($\lambda_{2,3}$), ADC and FA values. The ADC values increase and the FA values decrease as the fraction of the water compartment increases. All of the (**D**,*f*) couples perfectly fit the synthetic measurements including those that have negative eigenvalues (FA and ADC are not calculated for the negative tensors). This shows that the fitting problem is ill-posed since there is more than one possible solution, and that without constraining, the results can be nonphysical.

determines a single unique tensor that solves the DTI inverse problem for any $\widehat{\mathbf{A}}_t$ (21); this is also the solution for the inverse problem of the bi-tensor model for a given *f*. We can therefore choose any arbitrary value in the range $0 < f \leq 1$ and for each such value find its fitting tensor (Table 1), resulting in infinite (*f*,**D**) couples. For a general HARDI acquisition a set of overdetermined equations has to be fitted to the six tensor parameters (20). The fitting then depends on a minimization criterion (for instance, least squares). But since the measurements are noisy, it is highly unlikely that there is a solution with a perfect fit. Hence the (*f*,**D**) couples become local minima, among which the global minimum will be determined according to the noise type and fitting method selection. Practically all of the (*f*,**D**) local minima can be selected to solve the bi-tensor inverse problem, and choosing among them requires additional constraints.

Adding Constraints to the Bi-tensor Model Fitting

In order to stabilize the fitting process by reducing the number of possible solutions, we suggest incorporating restrictions on the desired solution. The restrictions are added to a variational framework and are based on biological or physical limitations that are not part of the bi-tensor model itself.

Variational Framework for the Bi-tensor Model

The solution for the inverse problem is restricted to show piece-wise smooth continuity between neighboring voxels. This restriction reflects the continuous property of diffusivities in an area that contains the same tissue. We would expect the tissue compartment to have smooth variations of tensor values between neighboring voxels, unless those voxels belong to different tissue types (22,23). The restriction is added to the bi-tensor model fitting by using a variational regularization framework (24) that defines the following functional, and minimizes it:

$$\mathrm{L}(\mathbf{D},f) = \int_{\Omega} \left(\left\| \mathbf{A}_{\text{bi-tensor}}(\mathbf{D},f) - \widehat{\mathbf{A}} \right\| + \alpha \sqrt{|\gamma(\mathbf{D})|} \right) d\Omega. \quad [5]$$

The functional has two parts: the first part is called the model (or fidelity) term, and requires that the chosen solution fit the measured data to the bi-tensor model; the second part is the regularization term, and contains the Beltrami piece-wise smoothness constraint for the tissue compartment tensors. The relative influence of each term is controlled by a scalar, α. The Beltrami constraint (25) incorporates the Beltrami regularization operator (26) with an affine-invariant metric for diffusion tensors, which ensures that all operations remain in the positive-definite range (27). This is done by calculating distances on a high dimensional space combining the 3D image domain with the 6D feature space (the six tensor parameters), and projecting back to the image coordinates, via the induced metric, γ. The full expressions of the induced metric and the Beltrami operator are given in Appendix A2. Minimizing the volume of this metric ($|\gamma|$ denotes the determinant of γ) acts as a piece-wise smooth regularization operator that maintains important tissue discontinuities (26). The addition of a regularization term stabilized the ill-posed fitting problem (28), and the minimization could be performed in any selected way. We use gradient descent simultaneously on the entire image domain (all relevant voxels), σ. The solution is defined by an evolution equation for each parameter (the six tensor parameters and the volume fraction parameter) that dictates the value of the parameter at the next iteration, until reaching convergence. The evolution equations are given in Appendix A3.

Constraints Enforced on the Volume Fraction

The solution space is further narrowed by enforcing constraints on the volume fraction, which is initially limited to $0 < f \leq 1$. As shown above, selecting a value for *f* determines the corrected attenuation $\widehat{\mathbf{A}}_t$ (Eq. 4). Since $\widehat{\mathbf{A}}_t$ represents attenuation, it is physically limited to the range $0 \leq \widehat{\mathbf{A}}_t < 1$. This range can be further limited by the expected diffusivities of the tissue compartment: The diffusion in the tissue is expected to be hindered, so a $\lambda_{\max} < d$ threshold is set, and restricts $\widehat{\mathbf{A}}_t > \exp(-b\lambda_{\max}) \equiv A_{\min}$; the minimal diffusivity expected in the tissue, $\lambda_{\min}$, restricts the maximal attenuation, hence, $\widehat{\mathbf{A}}_t < \exp(-b\lambda_{\min}) \equiv A_{\max}$. This dictates a new, restricted range for *f*:

$$f_{\min} \equiv \frac{\min(\widehat{\mathbf{A}}) - [\mathbf{A}_{\text{water}}]_k}{\mathbf{A}_{\min} - [\mathbf{A}_{\text{water}}]_k} < f < \frac{\max(\widehat{\mathbf{A}}) - [\mathbf{A}_{\text{water}}]_k}{\mathbf{A}_{\max} - [\mathbf{A}_{\text{water}}]_k} \equiv f_{\max} \quad [6]$$

where $\min(\widehat{\mathbf{A}})$ and $\max(\widehat{\mathbf{A}})$ are the minimal and maximal values in the vector $\widehat{\mathbf{A}}$. The new range, $f_{\min} < f < f_{\max}$, is calculated for each voxel.

MATERIALS AND METHODS

The framework was tested on two datasets, one from a healthy 32-year-old male volunteer and the other from a 40-year-old male patient with an extra-axial tumor (menin-

gioma) surrounded by massive edema. Both datasets were acquired with conventional DTI sequences. The dataset for the patient was taken as part of a clinical protocol and had a lower resolution (both in spatial and gradient orientation) than the volunteer's dataset. The entire analysis was performed with MatLab (MathWorks, Natick, MA) using an in-house tool called the diffusion imaging visualization and analysis (DiVa) toolbox, which is available online at http://www.cs.tau.ac.il/~oferpas/. The local Institutional Review Board approved the MRI protocols and informed consent was obtained from the subjects.

Imaging Parameters

The datasets were collected on a 3T scanner (GE, Milwaukee WI) using a diffusion-weighted spin-echo echo-planar-imaging (DWI-EPI) pulse sequence. The dataset for the healthy volunteer had the following parameters: Δ/δ = 30/24 ms; b = 1000 s/mm^2, with 19 noncolinear diffusion gradient orientations in addition to a nonweighted image ($\mathbf{S}_0$). The images acquired had a field of view (FOV) = 200 × 200 mm^2, over a 128 × 128 matrix, with 48 slices. Slice thickness was 2.5 mm, with no gap and a total scan time of about 10 minutes. The DW-EPI sequence was gated to the cardiac cycle with TR of 30 R-R intervals and TE of 88 ms.

The DW-EPI sequence for the tumor patient had the following parameters: TR/TE = 6000/78.5 ms; Δ/δ = 30/24 ms; b = 1000 s/mm^2, with six noncolinear diffusion gradient orientations in addition to an S_0 image. The images acquired had FOV = 240 × 240 mm^2, over a 128 × 128 matrix, with 24 slices. Slice thickness was 5 mm, with a 1-mm gap. The number of averages was 4, with a total scan time of about 3 minutes. In addition, the patient underwent a battery of clinical sequences, including T_2, FLAIR, and gadolinium-enhanced T_1.

DTI Analysis

All of the DWIs were coregistered using SPM2 (UCL, London, UK) to correct for head motion. Gradient orientations were compensated prior to the b-matrices calculation to account for the rotation component of the registration. The healthy dataset was further normalized to the MNI coordinates, using nonlinear deformations in SPM2, and compensating the gradients orientations for the rotation component of the affine-transformation that is the closest to the nonlinear deformations. DTI analysis was performed by the least-squares method (20), resulting in a tensor for each image voxel.

Bi-tensor Fitting

The bi-tensor fitting was performed by minimizing the functional Eq. [5]. The brain was segmented by applying a threshold on the $\mathbf{S}_0$ image. In addition, voxels identified by DTI to have eigenvalues larger than d (flow effects) or smaller than 0 were omitted. The minimization was performed iteratively on the entire remaining image using the gradient-descent method.

Initialization

An initial value for the volume fraction parameter, f, was selected as:

$$f_{t=0} = 1 - \frac{\log(\mathbf{S}_0/S_t)}{\log(S_w/S_t)} \quad [7]$$

where S_w is an intensity value from a voxel containing only a free water component (ADC ≅ d), and S_t is a baseline value from a voxel expected not to have a free water compartment (typically within deep white matter structures, with ADC ≅ 0.8). This initialization utilizes the fact that the $\mathbf{S}_0$ image is T_2-weighted and therefore shows high intensity at CSF and edema. Voxels where $f_{t=0} > f_{max}$ or $f_{t=0} < f_{min}$ were changed to the value $(f_{max} + f_{min})/2$.

Once the volume fraction parameter had been initialized, an initial guess for the tensor parameters of the tissue compartment was chosen by applying DTI on the free-water eliminated attenuation, $\widehat{\mathbf{A}}_t$ (Eq. [4]).

Iterations

The flow equations that dictate the gradient descent iteration are given in Appendix A3. Convergence was achieved in 100 iterations with $\alpha = 1$. We then set $\alpha = 0$ and ran 100 more iterations. The entire process required about 30 minutes to run on an AMD Opteron 250 workstation. The diffusivities were limited to λ_{max} = 2.5 mm^2/s and λ_{min} = 0.1 mm^2/s. Following each iteration, the new f values were monitored, and those that exceeded the limited range ($f < f_{min}$ or $f > f_{max}$ in Eq. [6]) were projected back. As a result, a tensor map modeling the free water eliminated tissue compartment was obtained. Mapping the weight of the water compartment (1-f) provided the free water maps.

Postprocessing and Visualization

The following analysis was performed separately on the tensor field obtained by DTI and on the free water eliminated tensor field found for the bi-tensor's tissue compartment. The tensors were spectrally decomposed to their eigen-components, and FA and ADC maps were calculated (3). The principal eigenvector from each voxel was used to draw a color-coded map (29). The intensities in the color-coded maps were attenuated by the FA values. The outcome of the two analysis methods was compared using FA-difference maps, which are voxel-wise subtractions of the FA derived by DTI from the FA of the tissue compartment tensor. Directionality difference maps were computed as the absolute angle between the orientation of the DTI derived tensor, i.e., its principal eigenvector, and the orientation of the tissue compartment tensor. In addition, tractography was applied using the principal eigenvectors and FA: the brute force FACT algorithm was used to generate the fiber coordinates (5), terminating at voxels with FA lower than 0.2 or following tract orientation change higher than 60°. Fibers that passed through a manually chosen seed region of interest (ROI) were plotted. The fibers were plotted as streamlines using MatLab. Once a subset of fibers had been found, a visitation map was generated, indicating voxels with at least one streamline passing through. The masks obtained were overlaid over the S_0 image.

Fornix Delineation

The fornix connects the hippocampus on each side of the brain with the mammillary bodies and septal nuclei. The

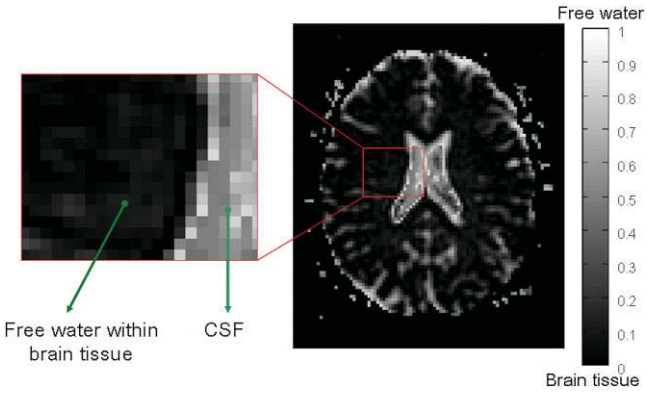

FIG. 1. Free water map: healthy subject. High intensities indicate a large volume of the free water compartment. Free water was found mostly in the CSF and around the brain parenchyma, and some within brain tissue (see inset). [Color figure can be viewed in the online issue, which is available at www.interscience.wiley.com.]

fornix body expected trajectory passes along the septum pellucidum, a membrane that separates the two lateral ventricles; its delineation is highly affected by CSF contamination (12–14). The fornix was reconstructed by manually selecting a seed ROI at the body of the fornix. Adjacent white matter structures (such as the cingulum) were screened out by restricting the fibers by a second ROI in proximity to the hippocampus. The presented streamlines are those that passed through both ROIs.

Corpus Callosum Delineation

The corpus callosum connects the left and right cerebral hemispheres and is the largest white matter structure in the brain. The posterior portion is called the splenium, the anterior the genu. The genu of the corpus callosum was reconstructed by selecting a single seed ROI on its midsagittal part.

RESULTS

CSF Contamination in the Healthy Subject

Figure 1 presents the free water map that was obtained by applying the bi-tensor fitting on the dataset from the healthy volunteer. High intensity values (approaching 1), reflecting a large volume of free water, were found for CSF voxels in the ventricles and around the brain parenchyma. Low values approaching 0 were found in gray and white matter areas. Values in the intermediate range identified voxels mainly at the CSF/brain tissue borderline. Small amounts of free water contamination were also found within deep white matter structures.

Figure 2 compares the ADC and FA-attenuated color-coded images obtained from DTI's tensor field (Fig. 2a,b) with those obtained from the water-eliminated tensor field (Fig. 2c,d). The images were very similar, with fine details and discontinuities in the DTI image preserved in the water-eliminated image. Differences in ADC were mostly in CSF-filled cavities around the brain parenchyma, and within and around the ventricles. The differences between the color-coded images are highlighted in the FA-difference map and in the directionality difference map (Fig. 2e,f). According to the FA-difference map (Fig. 2e), FA increased throughout many brain voxels, the increase was higher at CSF and white matter interfaces, and the increase was most prominent around and within the ventricles. According to the directionality difference map (Fig. 2f), high orientation differences (lower similarity) were found in areas expected to have CSF or gray matter voxels, and the differences in white matter voxels were minor (high directionality similarity).

The effect of free water elimination on tractography was demonstrated by reconstructing the fornix bundle (Fig. 3).

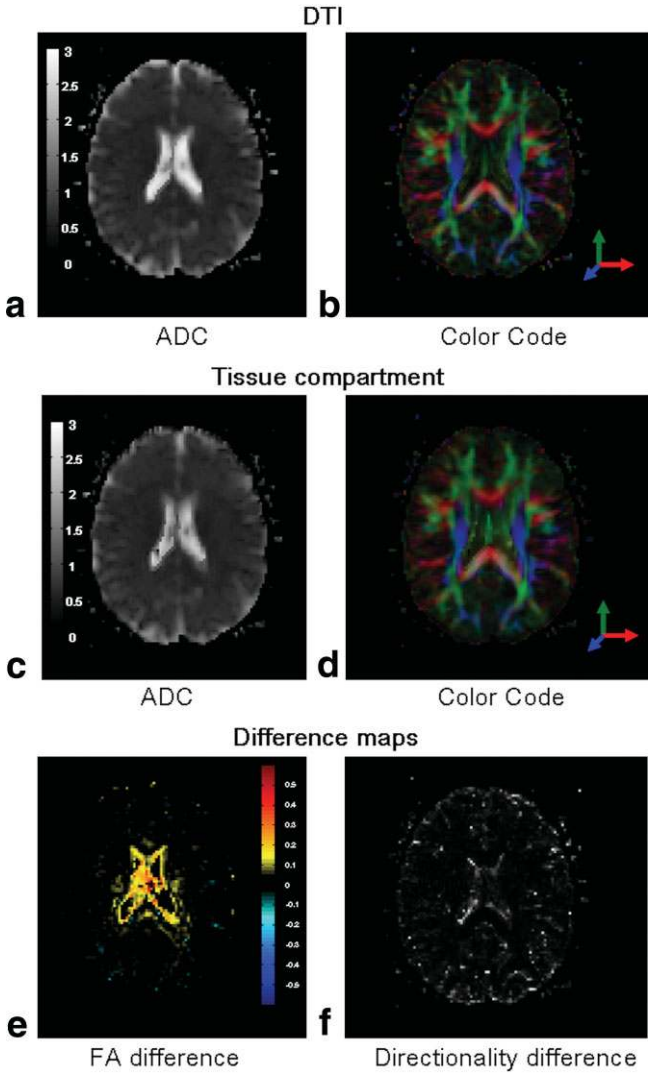

FIG. 2. Tissue compartment: healthy subject. ADC maps **(a,c)** and FA attenuated color-coded maps **(b,d)** representing the main diffusivity of the DTI results and the tissue compartment of the bi-tensor model are compared. The differences are highlighted in the FA-difference **(e)** (DTI subtracted from the tissue compartment) and orientation-difference **(f)** images. FA was elevated and ADC decreased mainly around the ventricles. Orientation was preserved throughout the brain tissue and was changed mainly in CSF voxels. This suggests that changes were selective to areas of partial volume, and preserved the quantities elsewhere. [Color figure can be viewed in the online issue, which is available at www.interscience.wiley.com.]

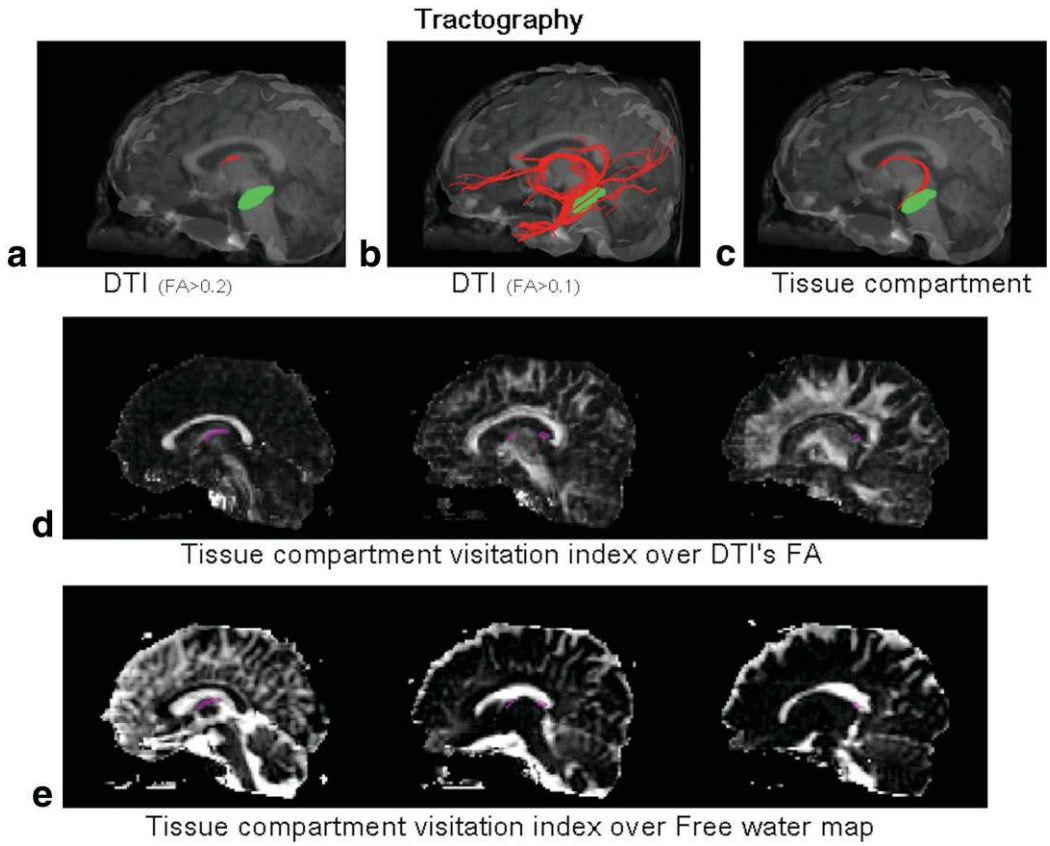

FIG. 3. Tractography: healthy subject. Comparison of the delineation of the fornix (red streamlines) using DTI **(a,b)** and using the tissue compartment obtained by the bi-tensor fit **(c)**. The hippocampus is shown for reference in green. The tract obtained by DTI with conventional FA threshold (0.2) preterminated at the body of the fornix **(a)**, while the bi-tensor fit tract delineated the entire route from the body of the fornix to its termination at the hippocampus. Lowering the FA threshold (FA $>$ 0.1) **(b)** results in a complete delineation of the fornix, yet with the cost of many false-positive streamlines. In **(d)** a magenta contour representing voxels where the bi-tensor tract passed is placed over a few sagittal FA slices of the DTI data, showing that the fiber passed in low FA voxels and caused the pretermination of the DTI tract. The same contour placed over the free water map **(e)** showed that the fiber passed right next to the ventricles in voxels with partial volume effect. [Color figure can be viewed in the online issue, which is available at www.interscience.wiley.com.]

For the DTI set, no fibers were found to connect the two ROIs; the reconstructed fiber from the fornix body ROI (Fig. 3a) showed a small part of the fornix and did not connect with the hippocampus. Lowering the FA threshold delineates the entire fornix (Fig. 3b), but the streamlines become too long, overlapping with adjacent white matter structure. The fiber reconstructed from the free water-eliminated tissue compartment (Fig. 3c) showed the full trajectory of the fornix to the hippocampus. Figure 3d presents the visitation maps for the free water-eliminated delineated fornix, superimposed over the FA map of the DTI data. Figure 3e shows the same contour placed on top of the free water map. These superimpositions show that the bi-tensor delineated route passed through partial volume voxels (high free water content), where DTI found FA values lower than the fiber tracking threshold. These voxels caused the premature termination of tracking with DTI, while free water elimination showed FA increase, which allowed the more complete delineation,.

Edema Contamination

The anatomical MRI for the clinical dataset (Fig. 4) revealed the presence of a tumor affecting the frontal lobe surrounded by a large volume of edema. As part of the clinical evaluation, the tumor and edema were manually segmented by an expert. Two slices of this dataset are presented in Figs. 5–8.

The free water maps (Figs. 5, 7c) showed that the entire area of the edema had partial volume of a free water compartment with a mean fractional volume of 0.45 $\pm$ 0.15. The mean fractional volume of the water compartment of the tumor area was 0.19 $\pm$ 0.08, and that of the rest of the gray/white matter was 0.10 $\pm$ 0.13. Areas not affected by the edema showed findings similar to the free water maps of the healthy volunteer: high contrast at CSF, low at brain tissue, and intermediate values on the interface between them. Free water intensity within deep white matter was again found, more widespread than for the healthy volunteer. The FA, ADC, and orientation changes in the normal appearing tissue were the same as those seen in the healthy subject.

The ADC of the DTI analysis (Fig. 6a) for the area of the edema (cyan contour) was hyperintense, while the ADC of the tissue compartment (Fig. 6c) had values similar to the rest of the brain. The DTI color-coded images (Figs. 6b, 7a) showed reduced FA for fiber bundles that passed through

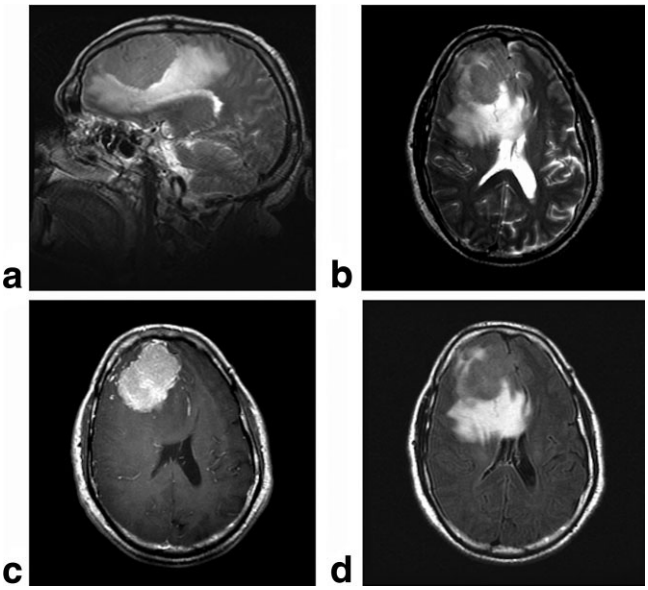

FIG. 4. Anatomy: edema. Anatomical images of a patient with a large tumor in the frontal lobe, surrounded by a large space-occupying edema. The extent of the lesion is seen in a mid-sagittal T_2 image **(a)** and in an axial slice **(b)** coregistered with the diffusion data. The extent of the tumor is best viewed in a gadolinium-enhanced T_1 image **(c)**, while the edema is best viewed with a T_2-FLAIR image **(d)**.

the edema compared to the intensity of unaffected white matter areas. Compared to the DTI values, the color-coded images for the tissue compartment derived from the bi-tensor fitting (Figs. 6d, 7b) showed elevated FA intensities within the edema, similar to those in unaffected areas (Table 2). The FA did not increase in the area of the tumor (yellow contour).

Scattering DTI's FA values relative to the tissue compartment FA showed that FA almost always increased (Fig. 8). The scatterplot was clustered using two linear criteria: $y = 0.45$ and $y = 1.6x$, to four distinct areas: low DTI's FA with low corrected FA values (blue); low DTI's FA with higher but lower-than-threshold corrected values (cyan); high DTI's FA with high corrected values (green); and low DTI's FA with high corrected FA values (light-green). Mapping these clusters back to the image domain revealed segments within the edema (Fig. 8a,b), a segmentation that could not be seen with anatomical MRI such as FLAIR (Fig. 8c,d).

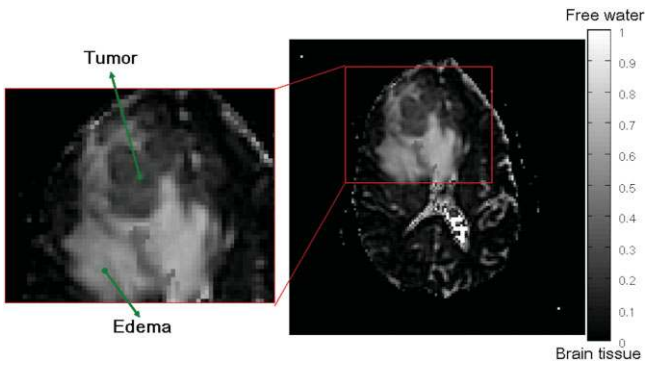

FIG. 5. Free water map: edema. The map allows segmentation of the edema and the tumor. The edema was detected as hyperintensity in the free water contrast (0.45 ± 0.15), while brain tissue showed lower intensities (0.1 ± 0.13). The tumor showed values in the range 0.19 ± 0.08. [Color figure can be viewed in the online issue, which is available at www.interscience.wiley.com.]

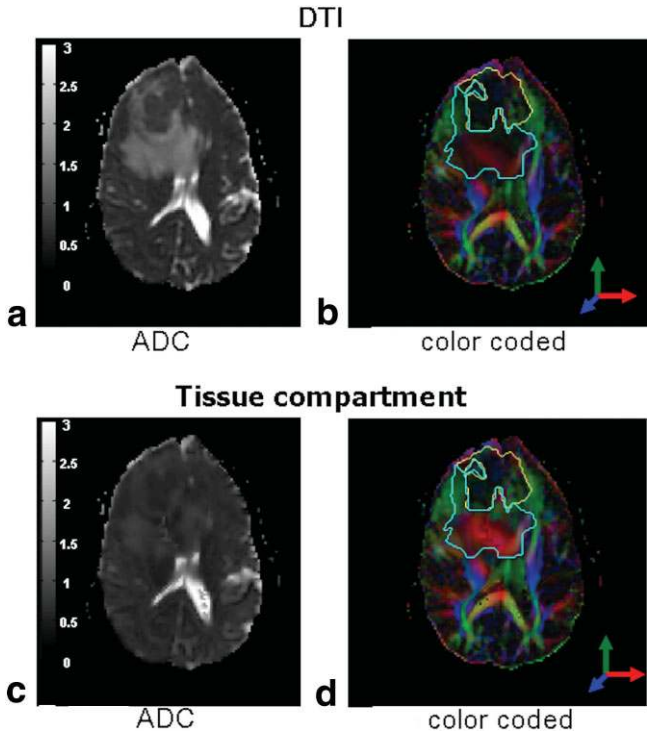

FIG. 6. Tissue compartment: edema. ADC maps **(a,c)** and color-coded maps **(b,d)** obtained by DTI (top row) and by the tissue compartment of the bi-tensor fit (bottom row) are compared. Most changes are within the edema area (cyan contour): ADC was hyperintense in DTI but was reduced following the free water removal. FA was selectively increased for the edematous area that contained white matter tracts, but was not increased in the area of the tumor (contoured with yellow). [Color figure can be viewed in the online issue, which is available at www.interscience.wiley.com.]

Performing tractography with the tensor field obtained by DTI (Fig. 9a), which showed poor cross-hemispheric connectivity at the genu of the corpus callosum, evidenced by no fiber traversing through the edema, suggested fiber degradation. Performing tractography on the tissue compartment tensor field derived from the bi-tensor fitting using the same seed ROI gave a different picture (Fig. 9b): the delineated tracts passed through the edema and crossed to the contralateral cortex. Laying a surface visualization of the tumor (shown as yellow surface) over the found tracts showed that the delineated fibers were most probably displaced by the tumor and passed close to its borders, but maintained cross-hemispheric connectivity. The crossing of the fibers through the edema was better visualized as an overlay of the fibers' visitation index on top of anatomical axial slices (Fig. 10): pixels were colored green if a DTI-derived tract went through them, and red if a tissue compartment-obtained tract went through them as well.

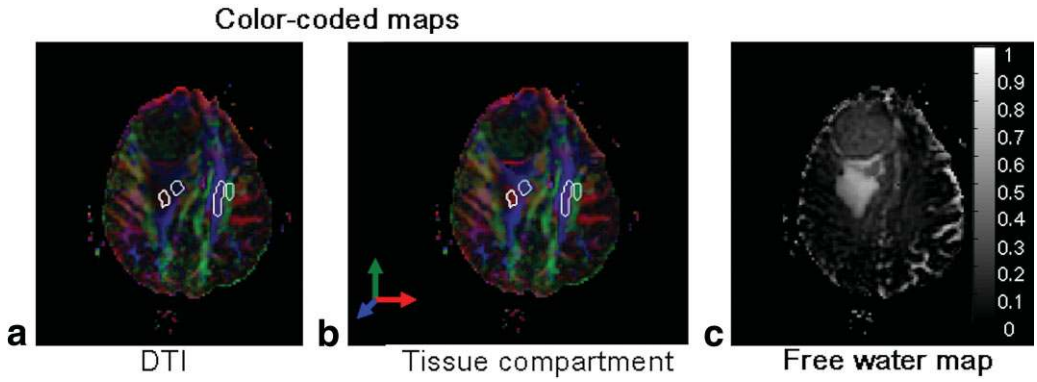

FIG. 7. Edema. The DTI color-coded map **(a)** shows a large area with decreased FA, suggesting fiber degradation due to the edema infiltration. The free water map **(c)** shows that the edema has high free water volume, while the tissue compartment derived from the bi-tensor fit **(b)** provides the additional information that FA values are similar to those on the unaffected side (see Table 2).

DISCUSSION

The main contribution of this study is an algorithm that extracts free water from diffusion MRI obtained by conventional DTI acquisitions, enabling better estimation of tissue-specific indices such as FA in areas of partial volume effect with CSF or edema, and more comprehensive fiber tracking in healthy and pathological conditions. We discuss below the effect of free water elimination on relating DTI indices to tissue microstructure, and the importance of the free water volume as a new imaging contrast. We also discuss model validation, implementation, and limitations issues concerning the bi-tensor model and the proposed minimization framework.

Imaging of Tissue Microstructure

One of the main benefits of diffusion imaging is that it provides microstructural information that can be related to processes within the tissue (3). The results suggest that diffusion indices derived from the free water-eliminated tissue compartment enhances the tissue specificity of the diffusion indices derived from DTI, especially for white matter delineation. In both the healthy and the tumor-patient datasets, FA values increase in areas expected to have partial volume of white matter with free water; the new FA values are similar to those in adjacent noncontaminated white matter voxels and better describe white matter geometry. An increase in FA is also observed within the ventricles and may reflect tissue residing within them (e.g., choroids plexus), or noise effect that becomes more apparent following removal of the free water. The corrected FA allows a more complete delineation of the fornix bundle. The fiber it discloses is very similar to fibers obtained by FLAIR-DWI (compare fig. 9 with fig. 4 in Ref. (14)), but it is obtained from a conventional DTI scan without the need for FLAIR.

Changes in the FA values within the edema following free water give valuable information about the underlying microstructure processes. While proximity to CSF does not change fiber diffusivities, vasogenic edema might

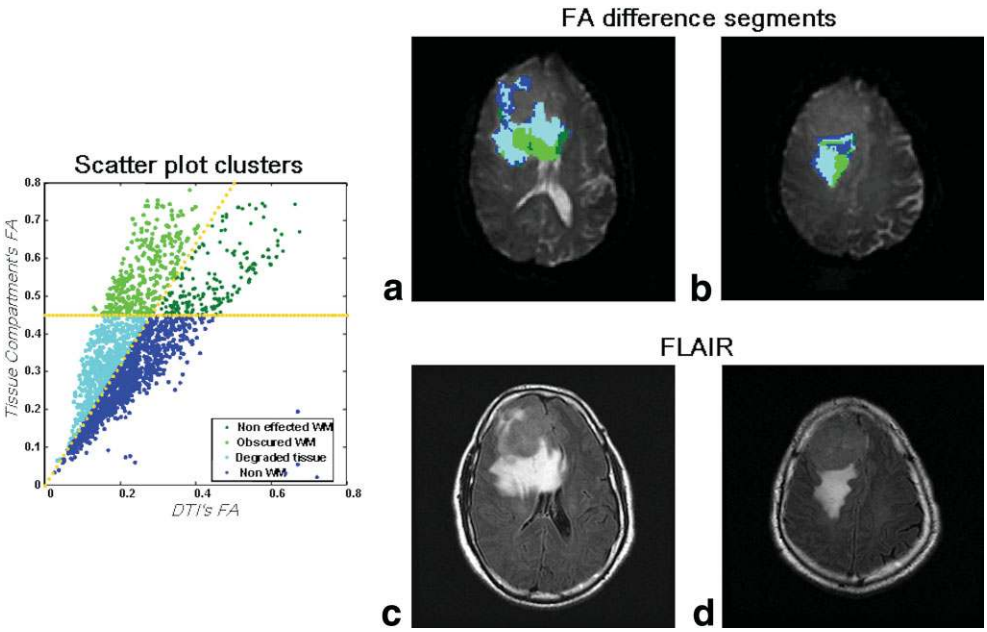

FIG. 8. Edema segmentation. By scattering DTI's FA against the corrected FA (left), the data appear to fall into four clusters which, when mapped back to the image domain **(a,b)**, reveal four segments within the edema. These segments imply the condition of the underlying tissue, and cannot be seen in anatomical contrast such as FLAIR **(c,d)**.

Table 2
Mean FA and ADC (Mean ± SD) Are Presented for the ROIs Contoured on Fig. 7

ROI4	ROI3	ROI2	ROI1	FA	ADC
0.4497 ± 0.0526	0.5151 ± 0.0619	0.1998 ± 0.0269	0.2261 ± 0.0371	DTI	DTI
0.4702 ± 0.0592	0.5687 ± 0.0595	0.4097 ± 0.0572	0.5092 ± 0.0229	Bi-tensor	Bi-tensor
0.0205 ± 0.0141	0.0535 ± 0.0192	0.2098 ± 0.0357	0.2831 ± 0.0510	Difference	Difference
0.6429 ± 0.0253	0.6790 ± 0.0393	1.2291 ± 0.0670	1.3073 ± 0.1421		
0.5989 ± 0.0156	0.5972 ± 0.0277	0.6425 ± 0.0208	0.6122 ± 0.0142		
−0.0440 ± 0.0222	−0.0818 ± 0.0266	−0.5866 ± 0.0617	−0.6951 ± 0.1450		

The ROIs are numbered from left to right, with ROI1 and ROI2 being contaminated by the edema. A much greater increase in FA and decrease in ADC are observed for the affected side (ROIs 1 and 2) following free water removal, and the values get closer to those on the unaffected side (ROIs 3 and 4).

cause tension on the fiber, change its density, or cause its degeneration (6), all of which clearly alter the diffusivities of the fiber bundle. Patterns of FA changes following the bi-tensor approach can characterize the effect of free water on partial volume of white matter and thereby indirectly characterize the underlying tissue:

1. An increase in FA within the affected region back to expected values suggests that no structural changes occurred to the fiber bundle in the region. Expected FA values may be those of the contralateral unaffected fiber, those along the fibers in areas unaffected by the edema, or ones known from the literature for the observed fiber.
2. A partial increase in FA (compared with expected values) suggests some degree of fiber degradation.
3. An FA increase above normal values may suggest thinning of the fibers due to the pressure applied by the edema on the fiber membranes (30).
4. No increase in FA in the affected area suggests that the underlying tissue is isotropic or the volume of the tissue is very small.

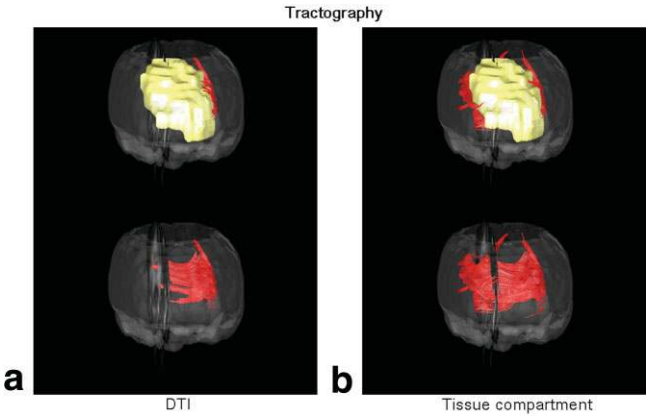

FIG. 9. Tractography: edema. Delineation of the corpus callosum from the DTI data showed no connectivity between hemispheres **(a)**, since the fiber terminated at the edematous area. Tractography using the tensor of the tissue compartment **(b)** on the same seed ROI crossed through the edema to the contralateral hemisphere. The yellow surface in the top panel visualizes the tumor, which seems to have pushed the colossal fibers (red streamlines). This can be seen in the bottom panel where the tumor surface is not rendered. [Color figure can be viewed in the online issue, which is available at www.interscience.wiley.com.]

The patterns of FA changes following the bi-tensor analysis can be related with the edema segments found in the tumor dataset (Fig. 8 and Table 2): the green segment is pattern #1, the cyan segment is pattern #2, and the blue segment is pattern #4. The segmentation according to patterns of FA-changes enables identification of underling tissue, not available with anatomical contrasts where the edema dominates the signal and is relatively homogenous, both in its T_2 and T_1 properties (Figs. 4, 8c,d), and in its relative volume (Figs. 5, 7c). The tissue segmentation within the edema is in line with the tractography results obtained by the bi-tensor fit (Fig. 9b) that show that the connectivity of the hemispheres in the damaged area is not completely lost, as suggested by the DTI tractography results (Fig. 9a). However, not all of the fibers were able to cross, suggesting that some degree of connectivity damage or fiber degradation did occur as a result of the edema infiltration, and the pressure caused by the space occupying tumor. Indeed, examination of the same patient after removal of the tumor and edema absorption indicated that the corpus callosum had recovered (data not shown).

Free Water Mapping

The ability to map the volume of free water introduces a new contrast mechanism that quantifies the partial volume within a voxel or the relative volume of free water. Estimating this parameter at the interface between CSF and brain tissue is important in order to eliminate free water contamination. However, as the results suggest, free water can also be found within the brain tissue itself, e.g., within deep white matter structures, where it may provide additional structural information. In the edema case, hyperintensities in the free water map are useful for delineating the area of the edema, suggesting an increase in the relative volume of the extracellular matrix. It is likely that the origin of the free water measure is from the extracellular matrix, since the cell size dictates a hindered displacement profile with diffusivity smaller than free water diffusivities (31). Similarly, we suggest that hyperintensities found in healthy-appearing brain tissue of both subjects indicate local accumulation of free water, which may be an important indication of the dynamics and condition of many processes. These could be any processes that involve changes in the relative volume of the intra- and extracellular space, such as maturation and aging, processes where water accumulation accompanies cell formation changes due to trauma, or degenerative processes like those that

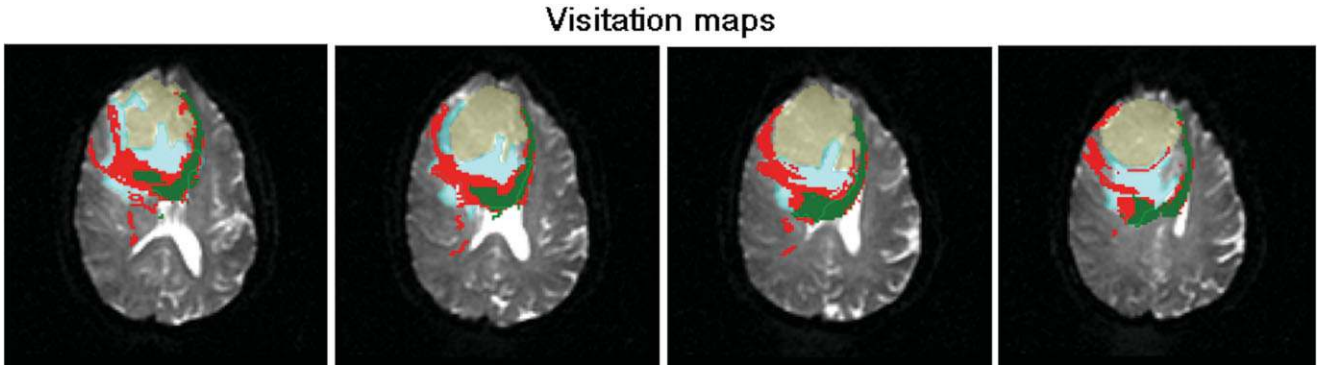

FIG. 10. Visitation index: edema. The visitation maps for the streamlines in Fig. 7 are plotted over four consecutive anatomical T_2 slices, where the tumor is yellow and the edema cyan. Green is for voxels where both the DTI obtained tract and the tissue compartment's tract passed. Red is where only the tissue compartment's tract passed. The DTI tract terminated at the edema, while the tissue compartment's tract continued to the opposite hemisphere, as was expected for the corpus callosum. [Color figure can be viewed in the online issue, which is available at www.interscience.wiley.com.]

occur in multiple sclerosis or cancer. The existence of free water within brain tissue is in line with previous findings by FLAIR-DWI, where small FA and ADC changes were identified (14).

The quantitative mapping of the volume of the water compartment is a main advantage of the bi-tensor approach over FLAIR-based CSF suppression methods. In addition, FLAIR-DWI suppresses only CSF free water (based on their T_1), but not edematous free water (that has a much shorter T_1). The volume of the free water compartment is a relative quantity and intrinsically limited to $0 < f \leq 1$, which makes the free water map a good candidate for cross-subject and cross-scan comparisons. As an alternative, free water within edematous tissue can be indirectly detected by hyperintensities in T_2-FLAIR, although these are dependent on scanning parameters and are hard to compare between subjects or across scans (32). For example, when examining excised tissues or tissue with variable temperature distribution, the extraction of free water can be done by fine-tuning the fitting parameters (the diffusion coefficient of the free water compartment), while the estimation of the free water fraction with FLAIR would necessitate changes at the acquisition level (33).

Model Validation

The problem of validating DTI results remains to be solved. There is no "ground truth" experiment available that truly models the diffusion properties of in vivo tissue, and there are great difficulties in comparing DTI indices with excised tissue (5). Nevertheless, when qualitative assessment of DTI indices are compared with prior anatomical and physiological information, the DTI indices in homogenous areas are in good agreement with the geometry of the tissue, and hence with its physiological properties (3,9). Validation of the bi-tensor model is therefore currently limited to comparing the diffusivities of the tissue compartment with the diffusivities obtained by DTI. The FA difference and directionality difference maps are the best validation tools in this case. It appears that FA is increased while directionality is preserved in free water-contaminated voxels compared to fibers in adjacent non-contaminated voxels. The sizes of the FA changes are similar to those recorded by FLAIR-DWI as reported (14): the 0.15–0.25 increase in FA in contaminated voxels in (14) is in line with the 0.2–0.28 increase reported here (ROIs 1 and 2 in Table 2); and a slight increase (0.02–0.05) of FA accompanied by a decrease of ADC (−0.04 to −0.08) is observed in less contaminated areas (ROIs 3 and 4 in Table 2 and the table in Ref. (14)). The latter FA increase may be explained by the existence of free water within the brain tissue. The free water signal is canceled with FLAIR-DWI sequence, and is calculated to have small values with the method described here; both yield a slight FA increase in the case of an underlying white matter. High directionality changes are found where the fitted tensor was expected to have low anisotropy within the ventricles and in some gray matter areas. In DTI the direction in those isotropic voxels is determined mainly by the direction of noise (3,9). Consequently, orientation changes for low anisotropy tensors hardly affect the fitting residual of the model term while at the same time they reduce discontinuities, and therefore are preferred by the minimization framework. The fact that directionality in white matter is preserved validates the fiber delineation results compared to the fibers delineated by DTI. In addition, the fibers obtained by eliminating free water appear more complete, and more closely resemble the expected anatomy. We note that the preservation of directionality implies that tracking through free water contaminated voxels could be achieved directly from the original tensor field by a global decrease of the FA threshold. This is indeed the case (Fig. 3b), but this approach has implications for non-CSF contaminated brain areas, which will have an overestimation of extracted tracts and a large number of false-positive fibers (5). Although we demonstrate here a single tractography approach (FACT), the implications of free water elimination are the same for any other fiber-tracking technique that is based on the shape of the diffusion tensor.

Implementation Issues

The tensor regularization scheme is based on the assumption of piece-wise smoothness of tensor elements. This

assumption was found appropriate for measures of physical quantities (34), and is especially useful in image processing and computer vision problems (35). The field of diffusion tensor regularization offers a variety of piecewise smoothed operators, all of which are based on the continuity assumption (e.g., (22–24,27) and (36) and references therein). The Beltrami operator selected here was recently shown to produce satisfactory results both in terms of quality and speed (25). It regularizes the entire tensor while preserving important image edges and remaining in a positive-definite space. In principle, any other regularization operator with these properties can be used as well.

The diffusion of information between neighboring voxels caused by smoothing is required to solve the ill-posed inverse problem. We previously used the extra information obtained by smoothing to fit tensors in areas of fiber ambiguity (37). There, as here, the piece-wise smooth regularization preserved fine details and discontinuities (Fig. 2.), suggesting that the regularization operator identifies neighboring tissues—including neighboring fiber pathways—as different.

In the context of free water elimination, acquiring smooth tracts is secondary to the estimation of the free water volume. The smoothing degree is controlled by the parameter α, but the absence of ground truth requires subjective assessment. In the application proposed here, once the volume fraction was found, we chose to deactivate the regularization term ($\alpha = 0$) and to continue the convergence for 100 more iterations. As a result, the outcome is not regularized explicitly and is less affected by the selection of α. Eliminating the smoothing effect also enables comparing the results with the nonregularized DTI results.

Tensor Model Limitations

The proposed framework was designed to be included in the existing DTI pipelines. As such, the DWIs are acquired with conventional DTI sequences, which are nowadays available on most commercial clinical scanners and are part of regular clinical protocols. As with DTI, the proposed method requires at least six noncolinear diffusion gradients, and the model fit is improved as the number of gradients is increased (38). The fitted tissue compartment tensor then replaces DTI's tensor in any subsequent analysis. Because most commercial scanners offer DTI sequences, the interface with the DTI pipeline makes the proposed method very accessible. The method could even be retroactively applied on any DTI dataset.

The tensor approach does, however, have some limitations. The first is the assumption that there is no exchange of water molecules between compartments; the exchange rate of different brain tissues and its effect on the tensor model are open questions (39). In this context, special care has to be taken with edema, since it might be correlated with changes in tissue permeability (40). An increase in the exchange rate is expected to cause an increase in bulk diffusivity and a decrease in FA for regular DTI analysis. In the bi-tensor model, it is expected to cause a bias in the estimation of the free water volume, and therefore a bias in the FA values of the tissue compartment. The same limitation applies to processes that occur in gray matter, where the cell bodies are more permeable than the myelin sheets of the fiber bundles (41). Another limitation of the tensor model is that it does not account for the non-Gaussian part of the diffusion decay (42). There is no doubt that at higher b-values the removal of the free water effect is easier because of its fast attenuation (18). But the analysis of the remaining signal has to be performed with more sophisticated models that account for non-Gaussianity. Preliminary results demonstrate that eliminating the free water compartment simplifies and enhances the Axcaliber model (43), and the CHARMED model (31), compartmental models that account for non-Gaussianity. Free water elimination is also expected to improve nonmodel-based diffusion imaging methods, such as q-ball (44) and pasMRI (45), which estimate an orientation distribution function (ODF). Eliminating the free water does not change the orientation of the peaks in the ODF, but at the same time those peaks become more prominent, allowing a more robust identification. We note that peaks that are noise related will be emphasized as well, and therefore incorporating free water elimination requires the use of regularization during the ODF estimation (46).

Pulsation artifact is a problem for correct estimation of FA in DTI (17), and the same problem remains when using the bi-tensor fit (in a nongated experiment). The biased anisotropy will not be included in the isotropic part and hence has the potential to affect the tissue compartment. But because the bi-tensor fitting is nonlinear and regularized, the biased FA may also remain in the fitting residual. This will happen if the regularization is turned on ($\alpha > 0$), in which case the tissue compartment will be regularized with normal-appearing white matter, and the minimization will favor a similar FA.

Because the bi-tensor model considers the T_1 and T_2 of both compartments to be the same, the free water volume estimations are T_1- and T_2-weighted (Appendix A1), and may not reflect the real ratio between the compartments. This bias, which depends on scanning parameters, may be eliminated by incorporating T_1 and T_2 maps acquired separately.

The assumption that edema has the same diffusion properties as free water may not be correct. At this time we use a fixed value for the diffusivity of the edema based on the fact that vasogenic edema is mainly composed of water and is trapped in the extracellular matrix (6). But it is possible that edema has slightly different diffusivities than free water, and that different types of edema have different diffusivities. As a result the obtained volume fractions may be biased and may yield biased diffusivities of the tissue compartment. In any case, they are less biased than the noncorrected DTI diffusivities. Adding the diffusivity of the water compartment as a free parameter (47) may reduce this bias, but at the cost of lengthier computation and a less stable minimization process. We find that the diffusivities of the tissue compartment are less susceptible to changes in the water compartment diffusivities than the volume fraction parameter, probably because the regularization applied on the tissue compartment maintains its eigenvalues in a certain range.

CONCLUSIONS

When inferring tissue structure from diffusion quantities it is important that the measures be specific for the tissue. In this work we propose a method that obtains enhanced diffusion indices for the case of partial volume with free water. Using the bi-tensor separation together with additional biological and physical constraints, we demonstrated that it is possible to differentiate the contribution of the free water compartment from that of the tissue compartment. Mapping the free water is also important in order to estimate the extracellular volume that is changed due to several processes. This map can be a valuable contrast tool in cross-subject and cross-scan analyses. We therefore suggest that free water elimination be performed as preprocessing for any DTI-related analysis, both in healthy and clinical cases.

ACKNOWLEDGMENTS

The authors thank Ms. Efrat Sasson for acquiring the data and Dr. Carlo Pierpaoli for helpful discussions.

APPENDIX

A1. Bi-tensor Model as a Special Case of the Multiple Tensors Model

The multiple diffusion tensors (MDT) model assumes that each voxel contains n separate compartments where any i'th compartment is modeled by a diffusion tensor $\mathbf{D}_i$ as:

$$[\mathbf{A}_i(\mathbf{D}_i)]_k = \exp(-b\mathbf{q}_k^{\mathrm{T}}\mathbf{D}_i\mathbf{q}_k). \quad [A1]$$

The overall attenuation for a given gradient direction is the weighted mean of all compartments, where each compartment contributes according to its weight f_i, ($0 < f_i < 1$, $\sum_{i=1}^{n} f_i = 1$):

$$\mathbf{A}_{\mathrm{MDT}}(\mathbf{D}_1,\cdots,\mathbf{D}_n,f_1,\cdots,f_n) = \sum_{i=1}^{n} f_i\mathbf{A}_i(\mathbf{D}_i). \quad [A2]$$

The weights are proportional with the volume (the number of molecules, m_i) of each compartment and are weighted by the T_1 and T_2 of each compartment:

$$f_i = \frac{m_i\exp(-TE/(T2)_i)(1-\exp(-TE/(T1)_i)}{\sum_{j=1}^{n} m_j\exp(-TE/(T2)_j)(1-\exp(-TE/(T1)_j)} \quad [A3]$$

If considering the same T_1 and T_2 in all compartments, then f_i is the volume fraction parameter. In order to account for CSF contamination, we assume that one of the compartments is a free water compartment with the attenuation $\mathbf{A}_{\mathrm{water}}$. The MDT model is therefore extended to:

$$\mathbf{A}_{\mathrm{MDT}} = \sum_{i=1}^{n} f_i\mathbf{A}_i + \left(1 - \sum_{i=1}^{n} f_i\right)\mathbf{A}_{\mathrm{water}} \quad [A4]$$

and the bi-tensor model is then the case where a single compartment comprises all attenuations from the nonfree water compartments, i.e., $n = 1$. A regularization scheme for the MDT model was proposed in Ref. (37).

A2. Induced Metric

Here we provide details needed for implementation of the Beltrami framework (Eq. [5]) for a (six-dimensional) diffusion tensor field embedded in a nine-dimensional spatial-feature manifold. The general case of the Beltrami framework can be found in Ref. (26), and the general case of the diffusion tensor field embedding can be found in Ref. (25).

Denote by σ the three-dimensional image space and its metric, γ. Denote by M the nine-dimensional spatial-feature space combining the image manifold and the six-dimensional feature tensor manifold, and h denotes its metric. We can then define a mapping $\mathbf{X}:\boldsymbol{\Omega} \rightarrow M$. We refer to P_3 as the space of 3×3 symmetric positive-definite matrices. The infinitesimal distance on P_3 is defined by the natural Riemannian metric as follows: $ds^2 = \mathrm{trace}((\mathbf{Y}^{-1}d\mathbf{Y})^2)$, where $\mathbf{Y} \in P_3$ (27). To simplify the expression for ds^2, and the corresponding calculations, we parameterize the tensor with the Iwasawa coordinates using the Iwasawa decomposition (25):

$$\mathbf{Y} = \mathbf{N}^{\mathrm{T}}\mathbf{A}\mathbf{N} = \begin{pmatrix} 1 & 0 & 0 \\ x_4 & 1 & 0 \\ x_5 & x_6 & 1 \end{pmatrix}\begin{pmatrix} x_1 & 0 & 0 \\ 0 & x_2 & 0 \\ 0 & 0 & x_3 \end{pmatrix}\begin{pmatrix} 1 & x_4 & x_5 \\ 0 & 1 & x_6 \\ 0 & 0 & 1 \end{pmatrix} \quad [A5]$$

We use the Euclidean distance to measure distances between elements on the image manifold. Combining both distances into one metric we get the spatial-feature metric tensor:

$$h = \begin{pmatrix} 1 & 0 & 0 & 0 & 0 & 0 & 0 & 0 & 0 \\ 0 & 1 & 0 & 0 & 0 & 0 & 0 & 0 & 0 \\ 0 & 0 & 1 & 0 & 0 & 0 & 0 & 0 & 0 \\ 0 & 0 & 0 & \frac{1}{x_1^2} & 0 & 0 & 0 & 0 & 0 \\ 0 & 0 & 0 & 0 & \frac{1}{x_2^2} & 0 & 0 & 0 & 0 \\ 0 & 0 & 0 & 0 & 0 & \frac{1}{x_3^2} & 0 & 0 & 0 \\ 0 & 0 & 0 & 0 & 0 & 0 & \frac{2x_1(x_3 + x_2x_6^2)}{x_2x_3} & -\frac{2x_1x_6}{x_3} & 0 \\ 0 & 0 & 0 & 0 & 0 & 0 & -\frac{2x_1x_6}{x_3} & \frac{2x_1}{x_3} & 0 \\ 0 & 0 & 0 & 0 & 0 & 0 & 0 & 0 & \frac{2x_2}{x_3} \end{pmatrix} \quad [A6]$$

We then project this metric back to the image domain to get the induced metric. The components of the induced metric are given as (written with the Einstein summation convention):

$$\gamma_{\mu\nu}(x) = \partial_\mu\mathbf{X}^i\partial_\nu\mathbf{X}^j\mathrm{h}_{ij}(\mathbf{X}). \quad [A7]$$

The indices μ and ν take the values 1, 2, or 3. The coordinates of the spatial-feature space are denoted by $\mathbf{X}^i$, and the indices i and j take the values 1 to 9.

A3. Gradient Descent Scheme

Solving the Euler–Lagrange equation for Eq. [5] (given the explicit definition in Eq. [A6]) provides the iteration rules toward the regularized tensor parameters. Since we use a Cartesian image grid, the $\mathbf{X}^i$ coordinates for i = 1, 2, 3 are simply the grid coordinates. The remaining six dimensions correspond to the six Iwasawa parameters, and are found iteratively using the step rules (written with the Einstein summation convention):

$$\mathbf{X}_t^i = -\alpha b \frac{1}{\sqrt{|\gamma|}} \sum_{k=1}^{n} (\mathbf{A}_{\text{bi-tensor}} - \widehat{\mathbf{A}}) \mathbf{A}_{\text{tissue}} \left(\mathbf{q}_k^{\mathrm{T}} \frac{\partial \mathbf{D}}{\partial \mathbf{X}_i} \mathbf{q}_k \right) + \frac{1}{\sqrt{|\gamma|}} \partial_\mu \sqrt{|\gamma|} (\gamma^{\mu\nu} \partial_\nu \mathbf{X}^i) + \mathbf{\Gamma}_{jk}^i \gamma^{\mu\nu} \partial_\mu \mathbf{X}^j \partial_\nu \mathbf{X}^i \quad [A8]$$

where i takes the values 3,4,…,9 and $\gamma^{\mu\nu}$ is the inverse of the induced metric. The symbols $\mathbf{\Gamma}_{jk}^i$ are the Christoffel symbols defined by:

$$\mathbf{\Gamma}_{jk}^i = \frac{1}{2} \mathrm{h}^{il} (\partial_j \mathrm{h}_{lk} + \partial_k \mathrm{h}_{jl} + \partial_j \mathrm{h}_{jk}). \quad [A9]$$

The Christoffel numbers introduce a coupling between the Iwasawa parameters, which maintain the properties of the initial affine-invariant metric. Therefore, this scheme also maintains positive definite tensors throughout the iterations (25).

Calculating the partial derivative of the tensor over the Iwasawa coordinates is done using the Iwasawa decomposition (Eq. [A1]).

The iteration rule for the volume fraction is given as:

$$f_t = -b \sum_{k=1}^{n} (\mathbf{A}_{\text{bi-tensor}} - \widehat{\mathbf{A}})(\mathbf{A}_{\text{tissue}} - \mathbf{A}_{\text{water}}). \quad [A10]$$

For all the parameters we use Neumann boundary condition, and the initial conditions for any coordinate $\mathbf{X}^i$ are $\mathbf{X}_{[t=0]}^i = \mathbf{X}_0^i$.

REFERENCES

1. Stejskal E, Tanner JE. Spin diffusion measurements: spin echoes in the presence of a time-dependent field gradient. J Chem Phys 1965;42:288–292.
2. Basser PJ, Mattiello J, LeBihan D. MR diffusion tensor spectroscopy and imaging. Biophys J 1994;66:259–267.
3. Basser PJ, Pierpaoli C. Microstructural and physiological features of tissues elucidated by quantitative-diffusion-tensor MRI. J Magn Reson B 1996;111:209–219.
4. Assaf Y, Pasternak O. Diffusion tensor imaging (DTI)-based white matter mapping in brain research: a review. J Mol Neurosci 2008;34:51–61.
5. Mori S, van Zijl PC. Fiber tracking: principles and strategies — a technical review. NMR Biomed 2002;15:468–480.
6. Betz AL, Iannotti F, Hoff JT. Brain edema: a classification based on blood-brain barrier integrity. Cerebrovasc Brain Metab Rev 1989;1:133–154.
7. Papadopoulos MC, Saadoun S, Binder DK, Manley GT, Krishna S, Verkman AS. Molecular mechanisms of brain tumor edema. Neuroscience 2004;129:1011–1020.
8. Unterberg AW, Stover J, Kress B, Kiening KL. Edema and brain trauma. Neuroscience 2004;129:1021–1029.
9. Pierpaoli C, Basser PJ. Toward a quantitative assessment of diffusion anisotropy. Magn Reson Med 1996;36:893–906.
10. Pierpaoli C, Jezzard P, Basser PJ, Barnett A, Di Chiro G. Diffusion tensor MR imaging of the human brain. Radiology 1996;201:637–648.
11. Alexander AL, Hasan KM, Lazar M, Tsuruda JS, Parker DL. Analysis of partial volume effects in diffusion-tensor MRI. Magn Reson Med 2001;45:770–780.
12. Papadakis NG, Martin KM, Mustafa MH, Wilkinson ID, Griffiths PD, Huang CL, Woodruff PW. Study of the effect of CSF suppression on white matter diffusion anisotropy mapping of healthy human brain. Magn Reson Med 2002;48:394–398.
13. Chou MC, Lin YR, Huang TY, Wang CY, Chung HW, Juan CJ, Chen CY. FLAIR diffusion-tensor MR tractography: comparison of fiber tracking with conventional imaging. AJNR Am J Neuroradiol 2005;26:591–597.
14. Concha L, Gross DW, Beaulieu C. Diffusion tensor tractography of the limbic system. AJNR Am J Neuroradiol 2005;26:2267–2274.
15. Cercignani M, Inglese M, Pagani E, Comi G, Filippi M. Mean diffusivity and fractional anisotropy histograms of patients with multiple sclerosis. AJNR Am J Neuroradiol 2001;22:952–958.
16. Schonberg T, Pianka P, Hendler T, Pasternak O, Assaf Y. Characterization of displaced white matter by brain tumors using combined DTI and fMRI. Neuroimage 2006;30:1100–1111.
17. Pierpaoli C, Marenco S, Rohde G, Jones DK, Barnett AS. Analyzing the contribution of cardiac pulsation to the variability of quantities derived from the diffusion tensor. In: Proc 11th Annual Meeting ISMRM, Toronto; 2003:70.
18. Pierpaoli C, Jones DK. Removing CSF contamination in brain DT-MRIs by using a two-compartment tensor model. In: Proc 12th Annual Meeting ISMRM, Kyoto; 2004:1215.
19. Behrens TE, Woolrich MW, Jenkinson M, Johansen-Berg H, Nunes RG, Clare S, Matthews PM, Brady JM, Smith SM. Characterization and propagation of uncertainty in diffusion-weighted MR imaging. Magn Reson Med 2003;50:1077–1088.
20. Koay CG, Chang LC, Carew JD, Pierpaoli C, Basser PJ. A unifying theoretical and algorithmic framework for least squares methods of estimation in diffusion tensor imaging. J Magn Reson 2006;182:115–125.
21. Basser PJ, Pierpaoli C. A simplified method to measure the diffusion tensor from seven MR images. Magn Reson Med 1998;39:928–934.
22. Tschumperle D, Deriche R. Orthonormal vector sets regularization with PDE's and applications. Int J Comput Vis 2002;50:237–252.
23. Coulon O, Alexander DC, Arridge S. Diffusion tensor magnetic resonance image regularization. Med Image Anal 2004;8:47–67.
24. Pasternak O, Sochen N, Assaf Y. Variational regularization of multiple diffusion tensor fields. In: Weickert J, Hagen H, editors. Visualization and processing of tensor fields. Berlin: Springer; 2006.
25. Gur Y, Pasternak O, Sochen N. GL(n)-invariant framework for tensors regularization. Int J Comput Vis (in press).
26. Kimmel R, Sochen N, Malladi R. From high energy physics to low level vision. Scale-space theory in computer vision. Volume 1252. Lecture notes in computer science. Berlin: Springer; 1997. p 236–247.
27. Pennec X, Fillard P, Ayache N. A Riemannian framework for tensor computing. Int J Comput Vis 2006;66:41–66.
28. Aubert G, Kornprobst P. Mathematical problems in image processing: partial differential equations and the calculus of variations. Berlin: Springer; 2002.
29. Pajevic S, Pierpaoli C. Color schemes to represent the orientation of anisotropic tissues from diffusion tensor data: application to white matter fiber tract mapping in the human brain. Magn Reson Med 1999;42:526–540.
30. Assaf Y, Ben-Sira L, Constantini S, Chang LC, Beni-Adani L. Diffusion tensor imaging in hydrocephalus: initial experience. AJNR Am J Neuroradiol 2006;27:1717–1724.
31. Assaf Y, Basser PJ. Composite hindered and restricted model of diffusion (CHARMED) MR imaging of the human brain. Neuroimage 2005;27:48–58.
32. Wen W, Sachdev P. The topography of white matter hyperintensities on brain MRI in healthy 60- to 64-year-old individuals. Neuroimage 2004;22:144–154.

33. Tofts PS, Jackson JS, Tozer DJ, Cercignani M, Keir G, MacManus DG, Ridgway GR, Ridha BH, Schmierer K, Siddique D, Thornton JS, Wroe SJ, Fox NC. Imaging cadavers: cold FLAIR and noninvasive brain thermometry using CSF diffusion. Magn Reson Med 2008;59:190–195.
34. Alvarez L, Guichard F, Lions PL, Morel JM. Axioms and fundamental equations of image-processing. Arch Ration Mech Anal 1993;123:199–257.
35. Weickert J. Anisotropic diffusion in image processing. Stuttgart: Teubner; 1998.
36. Weickert J, Hagen H. Visualization and processing of tensor fields. Berlin: Springer; 2006.
37. Pasternak O, Assaf Y, Intrator N, Sochen N. Variational multiple-tensor fitting of fiber-ambiguous diffusion-weighted magnetic resonance imaging voxels. Magn Reson Imaging 2008;26:1133–1144.
38. Jones DK, Horsfield MA, Simmons A. Optimal strategies for measuring diffusion in anisotropic systems by magnetic resonance imaging. Magn Reson Med 1999;42:515–525.
39. Peled S. New perspectives on the sources of white matter DTI signal. IEEE Trans Med Imaging 2007;26:1448–1455.
40. Liu KF, Li F, Tatlisumak T, Garcia JH, Sotak CH, Fisher M, Fenstermacher JD. Regional variations in the apparent diffusion coefficient and the intracellular distribution of water in rat brain during acute focal ischemia. Stroke 2001;32:1897–1905.
41. Clark CA, Le Bihan D. Water diffusion compartmentation and anisotropy at high b values in the human brain. Magn Reson Med 2000;44:852–859.
42. Cohen Y, Assaf Y. High b-value q-space analyzed diffusion-weighted MRS and MRI in neuronal tissues — a technical review. NMR Biomed 2002;15:516–542.
43. Assaf Y, Blumenfeld-Katzir T, Yovel Y, Basser PJ. AxCaliber: a method for measuring axon diameter distribution from diffusion MRI. Magn Reson Med 2008;59:1347–1354.
44. Tuch DS, Reese TG, Wiegell MR, Wedeen VJ. Diffusion MRI of complex neural architecture. Neuron 2003;40:885–895.
45. Jansons KM, Alexander DC. Persistent angular structure: new insights from diffusion MRI data. Inverse Probl 2003;19:1031–1046.
46. Descoteaux M, Angelino E, Fitzgibbons S, Deriche R. Regularized, fast, and robust analytical Q-ball imaging. Magn Reson Med 2007;58:497–510.
47. Pasternak O, Sochen NA, Intrator N, Assaf Y. Neuronal fiber delineation in area of edema from diffusion weighted MRI. In: Weiss Y, Scholkopf B, Platt J, editors. Advances in neural information processing systems, 18, Cambridge, MA: MIT Press, 2006; p. 1075–1080.